INTERNATIONAL JOURNAL FOR NUMERICAL METHODS IN FLUIDS
*Int. J. Numer. Meth. Fluids* 2003; **43**:937–951 (DOI: 10.1002/fld.511)

# Parameter-uniform numerical methods for a laminar jet problem

Ali R. Ansari[1,*,†], Alan F. Hegarty[2,‡] and Grigori I. Shishkin[2,§]

[1]*Department of Mathematics & Statistics, University of Limerick, Limerick, Ireland*
[2]*Institute of Mathematics & Mechanics, Russian Academy of Sciences, Ural Branch, Ekaterinburg, Russia*

SUMMARY

We consider the classical problem of a two-dimensional laminar jet of incompressible fluid flowing into a stationary medium of the same fluid. The equations of motion are the same as the boundary layer equations for flow past an infinite flat plate, but with different boundary conditions. Numerical experiments show that, using appropriate piecewise-uniform meshes, numerical solutions together with their scaled discrete derivatives are obtained which are parameter (i.e., viscosity $\nu$) robust with respect to both the number of mesh nodes and the number of iterations required for convergence. While the method employed is non-conservative, we show with the aid of numerical experiments that the loss in conservation of momentum is minimal. Copyright © 2003 John Wiley & Sons, Ltd.

KEY WORDS: jet problem; boundary-layer equations; piecewise-uniform mesh; parameter-robust approximations

## 1. INTRODUCTION

For the numerical solution of many types of linear singular perturbationproblems, methods which are uniformly convergent with respect to the perturbation parameter were developed in References [1–3]. The key idea in these methods is the use of piecewise uniform meshes, which are appropriately condensed in the boundary layer regions. As part of an investigation into whether these ideas can be used for non-linear problems, in particular flow problems, we apply the technique to simple model problems, the exact solutions of which are available. Such a method was shown in Reference [4] to be uniformly convergent with respect to the perturbation parameter for the flat plate problem of Blasius [4, 5]. Here, we examine analogously the classical two-dimensional laminar jet problem [5]. Physically, a two-dimensional

* Correspondence to: A. R. Ansari, Department of Mathematics & Statistics, University of Limerick, Limerick, Ireland.
† E-mail: ali.ansari@ul.ie, web page: http://www.ul.ie/∼aransari
‡ E-mail: alan.hegarty@ul.ie, web page: http://www.ul.ie/∼ahegarty
§ E-mail: Grigorii@shishkin.ural.ru, web page: http://home.imm.uran.ru/SPP

Contract/grant sponsor: Enterprise Ireland; contract/grant number: SC-97-612, SC-98-612
Contract/grant sponsor: Russian Foundation for Basic Research; contract/grant number: 01-01-01022

*Received 20 April 2002*
*Revised 8 November 2002*

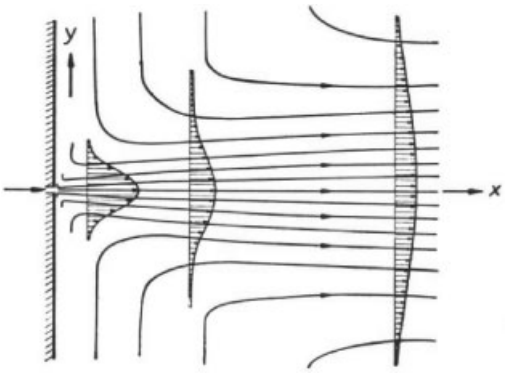


Figure 1. The two dimensional laminar jet (from [5]).

jet of incompressible fluid emerges from a narrow slit in a wall, which is assumed to be infinitesimal, into static medium of the same fluid (see Figure 1). In order to maintain a finite volume of flow as well as a finite momentum it is necessary to assume an infinite fluid velocity in the slit [5].

If the jet is thin, such that $u$ the horizontal component of velocity varies much more rapidly across the jet than along it, i.e. the $x$-axis, we have a boundary layer at $y=0$, i.e. the axis of the jet [6, 7]. The pressure gradient is zero in the jet since it is zero in the surrounding fluid. In the quarter plane

$$D=\{(x,y): x\geqslant 0,\ \ y\geqslant 0\} \tag{1}$$

the equations of motion are therefore the same as the Prandtl boundary layer equations [5], i.e.

$$\begin{aligned} -vu_{yy}+uu_x+vu_y&=0\\ u_x+v_y&=0 \end{aligned} \tag{2}$$

but with the different boundary conditions

$$\begin{aligned} u_y(x,0)=v(x,0)&=0 \quad \forall x>0\\ u(0,y)&=0 \quad \forall y>0\\ \lim u(x,y)&=0 \quad \text{for } x \text{ and/or } y\to\infty \end{aligned} \tag{3}$$

provided that

$$\int_{-\infty}^{\infty}\rho u^2\,\mathrm{d}y=J_0=\text{constant}$$

where $\rho$ is the density, $v$ in (2) is the viscosity.

The first equation of motion, involving the second derivative of $u$ and the viscosity $v$, is clearly a singularly perturbed differential equation with $v$ as the perturbation parameter. Our objective here is to obtain numerical solutions to this problem that are robust with respect to $v$. The sensitivity of classical numerical methods to the perturbation parameter is reflected in the maximum pointwise errors becoming unacceptably large for small $v$. This has been shown for

 

linear problems, e.g. in Reference [1] where it is also seen that inappropriate condensing of the mesh in the boundary layer region also fails to resolve the difficulty.

The approach adopted here comprises piecewise-uniform meshes [3], in conjunction with an upwind finite difference method, which lead to *parameter robust* numerical solutions, i.e. numerical solutions where the maximum pointwise error tends to zero independently of the perturbation parameter, while the work required to obtain the solutions is also independent of $v$. As the analytical solution of this particular problem is available we will use it to compute the discretization errors, always with respect to the discrete $L^\infty$ norm $\|\cdot\|_{\bar{\Omega}_v^N} = \max_{\bar{\Omega}_v^N} |\cdot|$.

It should be noted that Prandtl's boundary layer equations are valid approximations to the Navier–Stokes equations only for a small range of values of $v$. As there is no known *parameter robust* method for solving the Navier–Stokes equations, even for this simple geometry, it is worthwhile considering the solution of a simpler model. The problem under investigation here falls into this class. In addition, the range of values of $v$ that are employed here may appear unrealistic, since some of these fall outside the range of values that are physically valid for the model; however, the reason for the extended range of values here is to present a rigorous test of the robustness of the numerical method proposed. Numerical results will verify that this numerical method is indeed parameter robust.

## 2. THE ANALYTICAL SOLUTION

As mentioned in the previous section it is possible to obtain an analytical solution to the jet problem under consideration here [5–7]. The exact solutions $u$ and $v$ are

$$u \equiv \psi(x, y) = 6v\varphi^2 \frac{x}{y^2} \operatorname{sech}^2\varphi \tag{4}$$

$$v = 2v\varphi[2\varphi \operatorname{sech}^2\varphi - \tanh\varphi] \tag{5}$$

where

$$\varphi = \frac{1}{2}\left(\frac{1}{6}\right)^{1/3}\left(\frac{J_0}{\rho v^2}\right)^{1/3}\frac{y}{x^{2/3}}$$

Recall that $v$ is the viscosity, $\rho$ is the density and $J_0$ is the constant defined above, $J_0 = \int_{-\infty}^{\infty} \rho u^2 \, \mathrm{d}y$. Furthermore, some simple analysis [4, 5] shows that the thickness of the boundary layer $\xi$ is

$$\xi \sim \left(\frac{\rho v^2}{J_0}\right)^{1/3} x^{2/3} \tag{6}$$

Both $\rho$ and $J_0$ are constants and we set $\rho = J_0 = 1$ here.

## 3. THE NUMERICAL SOLUTION

We confine consideration to a finite rectangle

$$\Omega = (a, A] \times (0, B) \tag{7}$$

 

where the constants $a, A$ and $B$ are fixed and independent of the perturbation parameter $v$. We fix $a>0$ as the equations are singular at $x=0$ (this is apparent from (4) and (5)). Note that allowing $a$ to increase as $v\to 0$ would actually make the problem easier to solve as the computational domain would be far from the source. However, we require the method to work well on a *fixed domain for all* $v$, and thus fix $a$. We denote the boundary of $\Omega$ by $\Gamma=\Gamma_{\mathrm{L}}\cup\Gamma_{\mathrm{T}}\cup\Gamma_{\mathrm{B}}$ where $\Gamma_{\mathrm{L}}$, $\Gamma_{\mathrm{T}}$ and $\Gamma_{\mathrm{B}}$ denote the left, top and bottom edges of $\Omega$, respectively. We distinguish these boundaries from the right edge $\Gamma_{\mathrm{R}}=\{(x,y): x=A,\ y\in(0,B)\}$. Thus, it is required to find the solution of Equations (2) on $\Omega$ subject to the boundary conditions

$$u_y=0,\quad v=0\quad \text{on } \Gamma_{\mathrm{B}},\quad u=\psi\quad \text{on } \Gamma_{\mathrm{L}}\cup\Gamma_{\mathrm{T}} \tag{8}$$

where $\psi(x,y)$ is the analytical solution $u$ of the jet problem defined by (4).

We now define the computational mesh for this problem. On the rectangular domain $\bar{\Omega}$ we place the piecewise uniform rectangular mesh $\bar{\Omega}_v^{\mathbf{N}}$ which is the tensor product

$$\bar{\Omega}_v^{\mathbf{N}}=\bar{\Omega}^{N_x}\times\bar{\Omega}_v^{N_y} \tag{9}$$

where $\mathbf{N}=(N_x,N_y)$. Here $\bar{\Omega}^{N_x}$ is a uniform mesh over the interval $[a,A]$ with $N_x$ mesh intervals, while $\bar{\Omega}_v^{N_y}$ is a piecewise uniform fitted mesh with $N_y$ mesh intervals on the interval $[0,B]$. The interval $[0,B]$ is divided into two subintervals $[0,\sigma]$ and $[\sigma,B]$, $\sigma\leqslant B/2$, and $N_y/2$ uniform mesh intervals are assigned to each subinterval. Note that in Sections 3 and 4 we set $N_x=N_y=N$.

The transition point $\sigma$ is of significance as, by reducing $\sigma$ as $v$ decreases, the mesh in the $\sigma$-neighbourhood of the set $y=0$ will be condensed. The value of $\sigma$ is chosen, following the principles set out in References [2, 3] as

$$\sigma=\min\left\{\tfrac{1}{2}B,\ Cv^{2/3}\ln N\right\}$$

The choice of $v^{2/3}$ is motivated from (6), while $C$ is a constant independent of $v$, $N$ and $a$. Experimentation suggests the particular choice $C=2$ as a near optimal value which gives reasonable convergence rates for the iterative process.

We linearize the first equation by adapting the continuation algorithm set out in Reference [3] for the problem of flow past a flat plate. A monotone difference method is required, in particular for the jet problem, but we still encounter stability difficulties and thus need to generalize the algorithm from [1], as elaborated below. After linearization and discretization of (2) and the associated boundary conditions (8) we have the sequence of discrete linear problems for $m=0,1,\ldots$:

$$\begin{aligned} -v\delta_y^2 U_v^m(x_i,y_j)+\bar{U}_v^{m-1}D_x^- U_v^m(x_i,y_j)^m+\bar{V}_v^{m-1}D_y^{\pm}U_v^m(x_i,y_j)&=0\\ D_x^- U_v^m(x_i,y_j)+D_y^- V_v^m(x_i,y_j)&=0 \end{aligned} \tag{10}$$

with boundary conditions

$$\begin{aligned} D_y^0 U_v^m(x_i,y_0)=0,\quad V_v^m(x_i,y_0)=0\quad &\text{on } \Gamma_{\mathrm{B}}\cap\bar{\Omega}_v^{\mathbf{N}}\\ U_v^m(x_0,y_j)=u(x_0,y_j)\quad \text{on } \Gamma_{\mathrm{L}}\cap\bar{\Omega}_v^{\mathbf{N}},\quad U_v^m(x_i,y_N)=u(x_i,y_N)\quad &\text{on } \Gamma_{\mathrm{T}}\cap\bar{\Omega}_v^{\mathbf{N}} \end{aligned} \tag{11}$$

 

where

$$D_y^+ U_v^m(x_i, y_j) \equiv \frac{U_v^m(x_i, y_{j+1}) - U_v^m(x_i, y_j)}{y_{j+1} - y_j}$$

$$D_y^- U_v^m(x_i, y_j) \equiv \frac{U_v^m(x_i, y_j) - U_v^m(x_i, y_{j-1})}{y_j - y_{j-1}}$$

with analogous definition of $D_x^- U_v^m(x_i, y_j)$ and $D_y^- V_v^m(x_i, y_j)$,

$$D_y^0 U_v^m(x_i, y_j) \equiv \frac{U_v^m(x_i, y_{j+1}) - U_v^m(x_i, y_{j-1})}{y_{j+1} - y_{j-1}}$$

$$\delta_y^2 U_v^m(x_i, y_j) \equiv \frac{D_y^+ U_v^m(x_i, y_j) - D_y^- U_v^m(x_i, y_j)}{(y_{j+1} - y_{j-1})/2}$$

and where

$$D_y^{\pm} U_v^m(x_i, y_j) \equiv \begin{cases} D_y^- U_v^m(x_i, y_j) & \text{for } \bar{V}_v^{m-1}(x_i, y_j) > 0 \\ D_y^+ U_v^m(x_i, y_j) & \text{for } \bar{V}_v^{m-1}(x_i, y_j) < 0 \end{cases}$$

In addition,

$$\bar{U}_v^{m-1}(x_i, y_j) = (1 - \theta_1) U_v^{m-1}(x_i, y_j) + \theta_1 U_v^{m-2}(x_i, y_j)$$

$$\bar{V}_v^{m-1}(x_i, y_j) = (1 - \theta_2) V_v^{m-1}(x_i, y_j) + \theta_2 V_v^{m-2}(x_i, y_j)$$

where the parameters $0 \leqslant \theta_1,\ \theta_2 \leqslant 1$ and non-zero values are used to stabilize the iterative process as $v$ becomes smaller. The parameters can also affect the performance of the iterative process by increasing or decreasing iteration counts. In practice we always have $\theta_1 = \theta_2$; experimentation suggests that a near optimal value for these parameters is $\theta_1 = \theta_2 = 0.175$ for all $v$, which values are used in all the following numerical experiments. A detailed account of these parameters can be found in Reference [8].

## 4. NUMERICAL RESULTS

We (arbitrarily) set $a = 0.1$, $A = 1.1$ and $B = 1$, and the piecewise-uniform mesh for this problem, $\bar{\Omega}_v^{\mathbf{N}} \equiv \{(x_i, y_j)\}$, is then

$$x_i = x_{i-1} + h, \quad i = 1, \ldots, N, \quad x_0 = 0.1, \quad h = 1/N$$

$$y_j = \begin{cases} 2j\sigma/N, & j = 0, 1, 2, \ldots, N/2 \\ \sigma + 2(j - N/2)(1 - \sigma)/N, & j = N/2, \ldots, N \end{cases}$$

 

where

$$\sigma = \min\left\{\tfrac{1}{2},\ 2v^{2/3}\ \ln N\right\}$$

We can summarize the problem as

$$(P_v^{\mathbf{N}})\begin{cases}\text{Find } (U_v, V_v) \text{ such that } \forall (x_i, y_j) \in \Omega_v^{\mathbf{N}}\\ -v\delta_y^2 U_v^m(x_i, y_j) + \bar{U}_v^{m-1} D_x^- U_v^m(x_i, y_j) + \bar{V}_v^{m-1} D_y^{\pm} U_v^m(x_i, y_j) = 0\\ D_x^- U_v^m(x_i, y_j) + D_y^- V_v^m(x_i, y_j) = 0\\ D_y^0 U_v^m(x_i, y_0) = 0 \text{ and } V_v^m(x_i, y_0) = 0 \quad \text{on } \Gamma_{\mathrm{B}} \cap \bar{\Omega}_v^{\mathbf{N}}\\ U_v^m = u \quad \text{on } \{\Gamma_{\mathrm{L}} \cup \Gamma_{\mathrm{T}}\} \cap \bar{\Omega}_v^{\mathbf{N}}\end{cases} \tag{12}$$

The algorithm for solving $(P_v^{\mathbf{N}})$ sweeps across the domain $\Omega$ from $\Gamma_{\mathrm{L}}$ to $\Gamma_{\mathrm{R}}$. At the $i$th stage of the sweep, we compute the values of $(U_v, V_v)$ on $X_i = \{(x_i, y_j),\ 0 \leqslant j \leqslant N\}$, where $(U_v, V_v)$ are known on $X_{i-1}$. This is achieved by solving the first linearized equation for $U_v$, followed by a solution of the second linear equation for $V_v$.

In order to solve the first equation on $X_i$ we need values of $U_v$ on $X_{i-1}$, boundary values for $U_v^m$ on $\Gamma_{\mathrm{B}} \cup \Gamma_{\mathrm{T}}$ and an initial guess at $U_v^0$ on $X_i$. On each $X_i$, the 2 point boundary value problem for $U_v^m(x_i, y_j)$ is solved for $0 \leqslant j \leqslant N-1$. Since $U_v^m(x_i, y_0)$ is thus an unknown the term $D_y^{\pm} U_v^m(x_i, y_j)$ can and does introduce the value $U_v^m(x_i, y_{-1})$, which is eliminated by implementing the central difference approximation of the Neumann condition, so that all instances of $U_v^m(x_i, y_{-1})$ are replaced by $U_v^m(x_i, y_1)$. The initial guess to start the algorithm i.e. $U_v^0$ on $X_1$ is taken from the prescribed boundary condition for $U_v$ (the analytical solution) on $\Gamma_{\mathrm{L}}$. For each $X_i$, $V_v^0$ is set to be zero.

Once the solution to the tridiagonal system of equations for $U_v^m$ is obtained we then solve the linear system

$$D_x^- U_v^m(x_i, y_j) + D_y^- V_v^m(x_i, y_j) = 0, \quad 1 \leqslant j \leqslant N$$

for $V_v$. The process here is trivial as $U_v$ is known from the previous step and $V_v$ is initialized using the boundary condition, i.e. $V_v = 0$ on $\Gamma_{\mathrm{B}}$.

The iterative process is continued until a stopping criterion is achieved. This involves setting the tolerance tol, for the difference between two successive iterates, i.e.

$$\max(|U_v^{*\,m} - U_v^{*\,m-1}|_{\bar{\Omega}_v^{\mathbf{N}}},\quad |V_v^{*\,m} - V_v^{*\,m-1}|_{\bar{\Omega}_v^{\mathbf{N}}}) \leqslant \mathrm{tol}$$

where $U_v^{*\,m} = v^{1/3} U_v^m$, $V_v^{*\,m} = v^{-1/3} V_v^m$. We take tol to be $10^{-6}$. We let $m = M$ for all instances where the stopping criterion is met. Once this happens, we set $U_v = U_v^M$ and $V_v = V_v^M$ on $X_i$, and proceed to the next step $X_{i+1}$ using $U_v(x_i, y_j)$ as the initial guess for $U_v^m(x_{i+1}, y_j)$.

In Figure 2 we see the graphs of the numerical solution $U_v$ and a graph of the errors $|U_v - u|$ for $v = 2^{-10}$. The graph of the errors $|U_v - u|$ in Figure 2 highlights the differences and gives an idea of the accuracy. Similar graphs for $V_v$ and $|V_v - v|$ are shown in Figure 3. It is worth noting here that for this value of $v$ we require non-zero stability parameters $\theta_1$ and $\theta_2$ to aid the iterative process in convergence. In fact experimentally, for $v \leqslant 2^{-3}$, we require non-zero stability parameters.

To test the numerical solutions for $v$-uniform convergent, we consider some tables of errors and orders of convergence. The first of these tables, Table I, shows the normalized errors

 

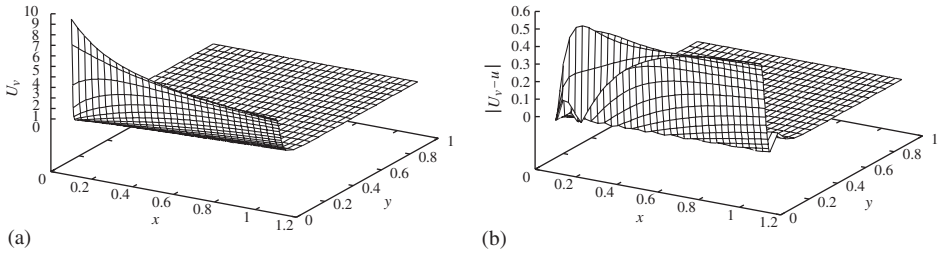


Figure 2. Surface plot of numerical solution $U_v$, is shown in (a). A plot of the error in the solution compared to the exact solution $|U_v - u|$, is shown in (b). Both plots are on $\Omega_v^{\mathbf{N}}$; $v = 2^{-10}$, $N = 32$, with stabilization factors $\theta_1 = \theta_2 = 0.175$.

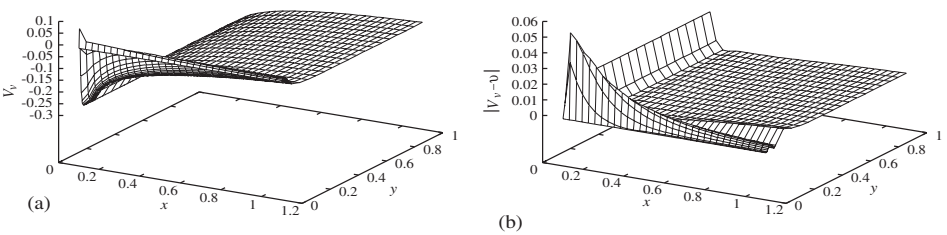


Figure 3. Surface plot of numerical solution $V_v$, is shown in (a). A plot of the error in the solution compared to the exact solution $|V_v - v|$, is shown in (b). Both plots are on $\Omega_v^{\mathbf{N}}$; $v = 2^{-10}$, $N = 32$, with stabilization factors $\theta_1 = \theta_2 = 0.175$.

Table I. Maximum pointwise errors, $E_v^N = \|U_v - u\|_{\bar{\Omega}_v^{\mathbf{N}}} / \|U_v\|_{\bar{\Omega}_v^{\mathbf{N}}}$, for various values of $v$ and $N$.

| | Number of intervals $N$ | | | | | |
|---|---|---|---|---|---|---|
| $v$ | 32 | 64 | 128 | 256 | 512 | 1024 |
| 1 | 0.992D − 02 | 0.589D − 02 | 0.321D − 02 | 0.168D − 02 | 0.857D − 03 | 0.433D − 03 |
| $2^{-1}$ | 0.194D − 01 | 0.107D − 01 | 0.559D − 02 | 0.287D − 02 | 0.146D − 02 | 0.733D − 03 |
| $2^{-2}$ | 0.245D − 01 | 0.130D − 01 | 0.672D − 02 | 0.342D − 02 | 0.173D − 02 | 0.867D − 03 |
| $2^{-3}$ | 0.282D − 01 | 0.148D − 01 | 0.759D − 02 | 0.385D − 02 | 0.194D − 02 | 0.973D − 03 |
| $2^{-4}$ | 0.346D − 01 | 0.179D − 01 | 0.909D − 02 | 0.459D − 02 | 0.230D − 02 | 0.115D − 02 |
| $2^{-5}$ | 0.456D − 01 | 0.231D − 01 | 0.116D − 01 | 0.581D − 02 | 0.291D − 02 | 0.145D − 02 |
| $2^{-6}$ | 0.571D − 01 | 0.327D − 01 | 0.166D − 01 | 0.830D − 02 | 0.415D − 02 | 0.207D − 02 |
| $2^{-7}$ | 0.571D − 01 | 0.339D − 01 | 0.197D − 01 | 0.112D − 01 | 0.622D − 02 | 0.315D − 02 |
| $2^{-8}$ | 0.571D − 01 | 0.339D − 01 | 0.197D − 01 | 0.112D − 01 | 0.622D − 02 | 0.342D − 02 |
| $2^{-9}$ | 0.571D − 01 | 0.339D − 01 | 0.197D − 01 | 0.112D − 01 | 0.622D − 02 | 0.342D − 02 |
| $2^{-10}$ | 0.571D − 01 | 0.339D − 01 | 0.197D − 01 | 0.112D − 01 | 0.622D − 02 | 0.342D − 02 |
| $R_{\text{unif}}^N$ | 0.75 | 0.78 | 0.82 | 0.85 | 0.86 | |

 

Table II. Maximum pointwise errors, $\|V_v - v\|_{\bar{\Omega}_v^N} / \|V_v\|_{\bar{\Omega}_v^N}$, for various values of $v$ and $N$.

| | Number of intervals $N$ | | | | | |
|---|---|---|---|---|---|---|
| $v$ | 32 | 64 | 128 | 256 | 512 | 1024 |
| 1 | 0.238D+00 | 0.127D+00 | 0.661D−01 | 0.338D−01 | 0.171D−01 | 0.859D−02 |
| $2^{-1}$ | 0.106D+00 | 0.563D−01 | 0.293D−01 | 0.149D−01 | 0.755D−02 | 0.380D−02 |
| $2^{-2}$ | 0.693D−01 | 0.375D−01 | 0.195D−01 | 0.992D−02 | 0.501D−02 | 0.252D−02 |
| $2^{-3}$ | 0.872D−01 | 0.468D−01 | 0.244D−01 | 0.124D−01 | 0.724D−02 | 0.413D−02 |
| $2^{-4}$ | 0.119D+00 | 0.646D−01 | 0.339D−01 | 0.207D−01 | 0.126D−01 | 0.700D−02 |
| $2^{-5}$ | 0.170D+00 | 0.949D−01 | 0.503D−01 | 0.340D−01 | 0.203D−01 | 0.112D−01 |
| $2^{-6}$ | 0.218D+00 | 0.138D+00 | 0.802D−01 | 0.542D−01 | 0.324D−01 | 0.178D−01 |
| $2^{-7}$ | 0.218D+00 | 0.140D+00 | 0.967D−01 | 0.744D−01 | 0.501D−01 | 0.282D−01 |
| $2^{-8}$ | 0.218D+00 | 0.140D+00 | 0.967D−01 | 0.744D−01 | 0.501D−01 | 0.308D−01 |
| $2^{-9}$ | 0.218D+00 | 0.140D+00 | 0.967D−01 | 0.744D−01 | 0.501D−01 | 0.308D−01 |
| $2^{-10}$ | 0.218D+00 | 0.140D+00 | 0.967D−01 | 0.744D−01 | 0.501D−01 | 0.308D−01 |
| $R^N_{\text{unif}}$ | 0.77 | 0.54 | 0.38 | 0.57 | 0.70 | |

$\|U_v - u\|_{\bar{\Omega}_v^N} / \|U_v\|_{\bar{\Omega}_v^N}$. We can clearly see from the table that the error is reducing along each row and the errors have stabilized down along each column of $N$. The table suggests $v$-uniform convergence as we have stability in the errors down each column of values of $N$ for the various values of $v$, and along each row we can see a trend of decreasing errors with rising $N$. In Table I—and analogously in subsequent tables—the uniform rates of convergence $R^N_{\text{unif}}$ for each $N$ are calculated as

$$R^N_{\text{unif}} = \log_2 \frac{E^N_{\max}}{E^{2N}_{\max}}$$

where $E^N_{\max} = \max_v E^N_v$. The computed uniform rates in Table I clearly reinforce the indicated $v$-uniform convergence of the numerical solutions.

The corresponding errors and the uniform rates of convergence for $V_v$ are given in Table II. The normalization in Table II is achieved by dividing the maximum absolute error by the maximum absolute value of $V_v$, for each set of values of $v$ and $N$ in the table.

There is a slight problem noticeable in Table II, which gives the uniform rates of convergence for $V_v$. Note that the rates are decreasing along each of the columns up to the column for $N = 128$, after which the trend reverses. This phenomenon does not occur for the flat plate problem [3]. This behaviour indicates the greater sensitivity of the laminar jet problem in comparison to the flat plate problem. This is further borne by the requirement to use non-zero values of the stability parameters $\theta_1$ and $\theta_2$ for the jet problem, which are not required for the flat plate problem.

## 5. APPROXIMATION OF THE DERIVATIVES

We wish to estimate the $x$ and $y$ derivatives of both the horizontal component of velocity $u$ and the vertical component of velocity $v$. Because of the presence of the boundary layer

 

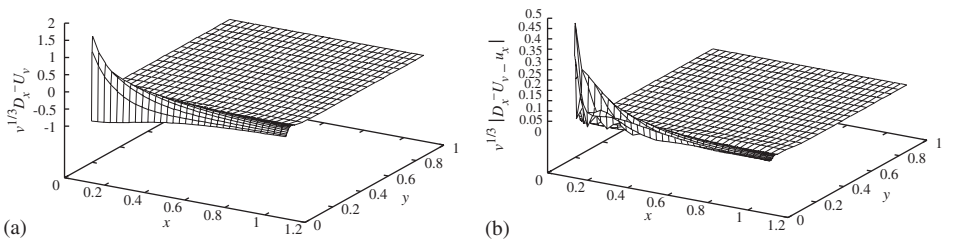


Figure 4. Surface plot of $v^{1/3}D_x^- U_v$, is shown in (a). A plot of the error $v^{1/3}|D_x^- U_v - u_x|$, is shown in (b). Both plots are on $\Omega_v^{\mathbf{N}}$; $v = 2^{-10}$, $N = 32$, with stabilization factors $\theta_1 = \theta_2 = 0.175$.

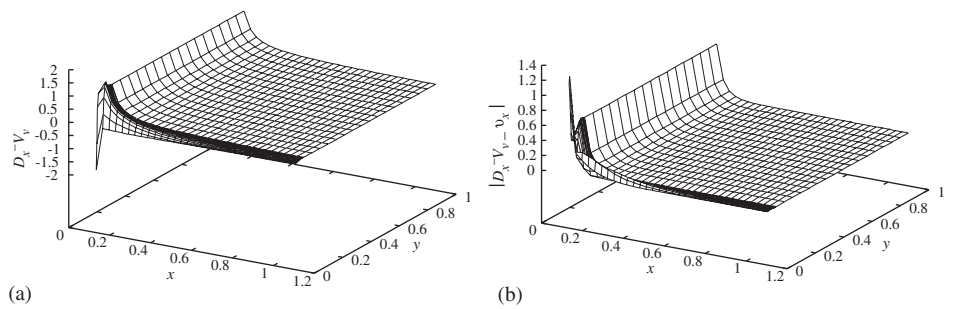


Figure 5. Surface plot of $D_x^- V_v$, is shown in (a). A plot of the error $|D_x^- V_v - v_x|$, is shown in (b). Both plots are on $\Omega_v^{\mathbf{N}}$; $v = 2^{-10}$, $N = 32$, with stabilization factors $\theta_1 = \theta_2 = 0.175$.

we have to scale the derivatives. The appropriate scaling is complex; each of the derivatives has to be considered separately. The derivative $u_x$ is scaled by a factor $v^{1/3}$, i.e. $v^{1/3}u_x$, which is approximated as $v^{1/3}D_x^- U_v$. The graphs of the approximation $v^{1/3}D_x^- U_v$ and of the error $v^{1/3}|D_x^- U_v - u_x|$ are shown in Figure 4.

The derivative $v_x$ does not require any scaling and is approximated as $D_x^- V_v$. The graphs of the approximation $D_x^- V_v$, and the error $|D_x^- V_v - v_x|$ are shown in Figure 5.

The derivative $u_y$ requires scaling, as for small values of $v$ the derivative is excessively large within the layer region. The appropriate scaling is $vu_y$, and the approximation is $vD_y^- U_v$. The graphs of $vD_y^- U_v$, and the error $v|D_y^- U_v - u_y|$ are shown in Figure 6.

The derivative $v_y$, is scaled by a factor $v^{1/3}$, i.e. $v^{1/3}v_y$, which is approximated as $v^{1/3}D_y^- V_v$. The graph of the approximation $v^{1/3}D_y^- V_v$ and the error $v^{1/3}|D_y^- V_v - v_y|$ are shown in Figure 7.

We now look at some error tables to judge the robustness of the approximations of the derivatives with respect to the perturbation parameter $v$. Note that all the errors could be stabilized by dividing by the maximum absolute value of the approximation of the respective derivative. However, since the approximation of the derivatives $u_x$ and $v_y$ should be scaled identically (because these two derivatives form the continuity equation in (2)), we will scale them by multiplying by a factor $v^{1/3}$, as used earlier.

The first of the results is given in Table III where we see the behaviour reflecting parameter robustness. In Table IV we see the errors in the approximation of the derivative $D_y^- U_v$. The

 

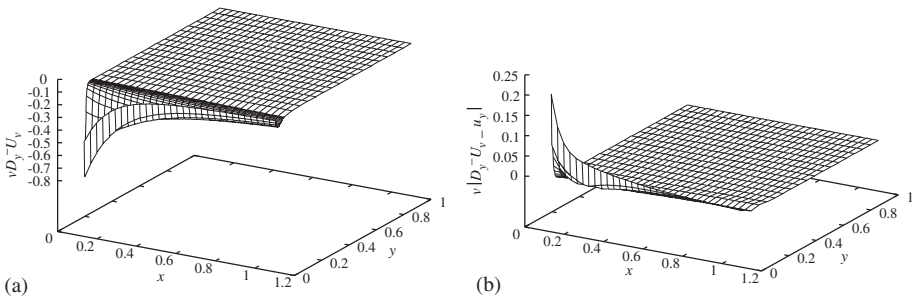


Figure 6. Surface plot of $vD_y^- U_v$, is shown in (a). A plot of the error $v|D_y^- U_v - u_y|$, is shown in (b). Both plots are on $\Omega_v^{\mathbf{N}}$; $v = 2^{-10}$, $N = 32$, with stabilization factors $\theta_1 = \theta_2 = 0.175$.

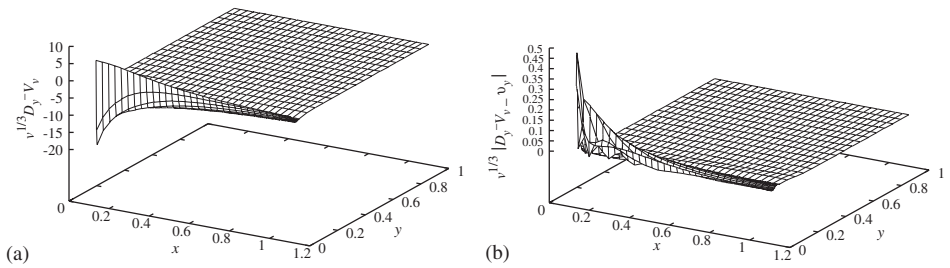


Figure 7. Surface plot of $v^{1/3} D_y^- V_v$, is shown in (a). A plot of the error $v^{1/3}|D_y^- V_v - v_y|$, is shown in (b). Both plots are on $\Omega_v^{\mathbf{N}}$; $v = 2^{-10}$, $N = 32$, with stabilization factors $\theta_1 = \theta_2 = 0.175$.

Table III. Maximum pointwise errors, $v^{1/3}\|D_x^- U_v - u_x\|_{\bar{\Omega}_v^{\mathbf{N}} \setminus \Gamma_L}$, for various values of $v$ and $N$.

| | Number of intervals $N$ | | | | | |
|---|---|---|---|---|---|---|
| $v$ | 32 | 64 | 128 | 256 | 512 | 1024 |
| 1 | 0.440D+00 | 0.238D+00 | 0.123D+00 | 0.620D−01 | 0.311D−01 | 0.156D−01 |
| $2^{-1}$ | 0.229D+00 | 0.127D+00 | 0.671D−01 | 0.346D−01 | 0.176D−01 | 0.885D−02 |
| $2^{-2}$ | 0.244D+00 | 0.135D+00 | 0.714D−01 | 0.368D−01 | 0.187D−01 | 0.942D−02 |
| $2^{-3}$ | 0.265D+00 | 0.148D+00 | 0.781D−01 | 0.403D−01 | 0.205D−01 | 0.110D−01 |
| $2^{-4}$ | 0.292D+00 | 0.166D+00 | 0.958D−01 | 0.589D−01 | 0.331D−01 | 0.177D−01 |
| $2^{-5}$ | 0.324D+00 | 0.245D+00 | 0.163D+00 | 0.966D−01 | 0.533D−01 | 0.282D−01 |
| $2^{-6}$ | 0.497D+00 | 0.447D+00 | 0.276D+00 | 0.158D+00 | 0.857D−01 | 0.450D−01 |
| $2^{-7}$ | 0.497D+00 | 0.474D+00 | 0.344D+00 | 0.223D+00 | 0.135D+00 | 0.717D−01 |
| $2^{-8}$ | 0.497D+00 | 0.474D+00 | 0.344D+00 | 0.223D+00 | 0.135D+00 | 0.784D−01 |
| $2^{-9}$ | 0.497D+00 | 0.474D+00 | 0.344D+00 | 0.223D+00 | 0.135D+00 | 0.784D−01 |
| $2^{-10}$ | 0.497D+00 | 0.474D+00 | 0.344D+00 | 0.223D+00 | 0.135D+00 | 0.784D−01 |
| $R_{\text{unif}}^N$ | 0.07 | 0.46 | 0.63 | 0.72 | 0.79 | |

 

Table IV. Maximum pointwise errors, $\|D_y^- U_v - u_y\|_{\bar{\Omega}_v^N \setminus \Gamma_L} / \|D_y^- U_v\|_{\bar{\Omega}_v^N \setminus \Gamma_B}$, for various values of $v$ and $N$.

| | Number of intervals $N$ | | | | | |
|---|---|---|---|---|---|---|
| $v$ | 32 | 64 | 128 | 256 | 512 | 1024 |
| 1 | 0.582D−01 | 0.346D−01 | 0.186D−01 | 0.974D−02 | 0.498D−02 | 0.252D−02 |
| $2^{-1}$ | 0.817D−01 | 0.411D−01 | 0.206D−01 | 0.103D−01 | 0.514D−02 | 0.257D−02 |
| $2^{-2}$ | 0.128D+00 | 0.651D−01 | 0.326D−01 | 0.163D−01 | 0.816D−02 | 0.408D−02 |
| $2^{-3}$ | 0.199D+00 | 0.103D+00 | 0.517D−01 | 0.259D−01 | 0.130D−01 | 0.648D−02 |
| $2^{-4}$ | 0.293D+00 | 0.160D+00 | 0.817D−01 | 0.411D−01 | 0.206D−01 | 0.103D−01 |
| $2^{-5}$ | 0.391D+00 | 0.243D+00 | 0.128D+00 | 0.651D−01 | 0.326D−01 | 0.163D−01 |
| $2^{-6}$ | 0.416D+00 | 0.354D+00 | 0.199D+00 | 0.103D+00 | 0.517D−01 | 0.259D−01 |
| $2^{-7}$ | 0.416D+00 | 0.368D+00 | 0.235D+00 | 0.141D+00 | 0.803D−01 | 0.411D−01 |
| $2^{-8}$ | 0.416D+00 | 0.368D+00 | 0.235D+00 | 0.141D+00 | 0.803D−01 | 0.448D−01 |
| $2^{-9}$ | 0.416D+00 | 0.368D+00 | 0.235D+00 | 0.141D+00 | 0.803D−01 | 0.448D−01 |
| $2^{-10}$ | 0.416D+00 | 0.368D+00 | 0.235D+00 | 0.141D+00 | 0.803D−01 | 0.448D−01 |
| $R_{\text{unif}}^N$ | 0.18 | 0.65 | 0.73 | 0.82 | 0.84 | |

Table V. Maximum pointwise errors, $v^{1/3}\|D_y^- V_v - v_y\|_{\bar{\Omega}_v^N \setminus \Gamma_B}$, for various values of $v$ and $N$.

| | Number of intervals $N$ | | | | | |
|---|---|---|---|---|---|---|
| $v$ | 32 | 64 | 128 | 256 | 512 | 1024 |
| 1 | 0.440D+00 | 0.238D+00 | 0.123D+00 | 0.620D−01 | 0.311D−01 | 0.156D−01 |
| $2^{-1}$ | 0.223D+00 | 0.126D+00 | 0.669D−01 | 0.346D−01 | 0.176D−01 | 0.885D−02 |
| $2^{-2}$ | 0.229D+00 | 0.133D+00 | 0.711D−01 | 0.367D−01 | 0.187D−01 | 0.942D−02 |
| $2^{-3}$ | 0.229D+00 | 0.142D+00 | 0.773D−01 | 0.402D−01 | 0.205D−01 | 0.110D−01 |
| $2^{-4}$ | 0.209D+00 | 0.152D+00 | 0.958D−01 | 0.589D−01 | 0.331D−01 | 0.177D−01 |
| $2^{-5}$ | 0.307D+00 | 0.245D+00 | 0.163D+00 | 0.966D−01 | 0.533D−01 | 0.282D−01 |
| $2^{-6}$ | 0.497D+00 | 0.447D+00 | 0.276D+00 | 0.158D+00 | 0.857D−01 | 0.450D−01 |
| $2^{-7}$ | 0.497D+00 | 0.474D+00 | 0.344D+00 | 0.223D+00 | 0.135D+00 | 0.717D−01 |
| $2^{-8}$ | 0.497D+00 | 0.474D+00 | 0.344D+00 | 0.223D+00 | 0.135D+00 | 0.784D−01 |
| $2^{-9}$ | 0.497D+00 | 0.474D+00 | 0.344D+00 | 0.223D+00 | 0.135D+00 | 0.784D−01 |
| $2^{-10}$ | 0.497D+00 | 0.474D+00 | 0.344D+00 | 0.223D+00 | 0.135D+00 | 0.784D−01 |
| $R_{\text{unif}}^N$ | 0.07 | 0.46 | 0.63 | 0.72 | 0.79 | |

appropriate scaling for the errors is achieved by dividing by $\|D_y^- U_v\|_{\bar{\Omega}_v^N}$. It is quite clear that the errors are reducing along the rows, and they have stabilized down along each of the columns. In addition, Table IV also shows the uniform rates of convergence. These tables reflect $v$-uniform convergence.

The next table, i.e. Table V also shows $v$-uniform behaviour.

The next set of tables are for $D_x^- V_v$, where a difficulty arises. It is clear that the errors have stabilized down along each of the columns. The correct scaling for achieving this stabilization

 

Table VI. Maximum pointwise errors, $\|D_x^- V_v - v_x\|_{\bar{\Omega}_v^N \setminus \Gamma_L} / \|V_v\|_{\bar{\Omega}_v^N \setminus \Gamma_L}$, for various values of $v$ and $N$.

| | Number of intervals $N$ | | | | | |
|---|---|---|---|---|---|---|
| $v$ | 32 | 64 | 128 | 256 | 512 | 1024 |
| 1 | 0.371D+01 | 0.279D+01 | 0.326D+01 | 0.311D+01 | 0.280D+01 | 0.248D+01 |
| $2^{-1}$ | 0.144D+01 | 0.934D+00 | 0.112D+01 | 0.136D+01 | 0.147D+01 | 0.153D+01 |
| $2^{-2}$ | 0.142D+01 | 0.107D+01 | 0.142D+01 | 0.163D+01 | 0.172D+01 | 0.177D+01 |
| $2^{-3}$ | 0.126D+01 | 0.185D+01 | 0.228D+01 | 0.270D+01 | 0.361D+01 | 0.418D+01 |
| $2^{-4}$ | 0.236D+01 | 0.315D+01 | 0.371D+01 | 0.510D+01 | 0.635D+01 | 0.711D+01 |
| $2^{-5}$ | 0.407D+01 | 0.508D+01 | 0.601D+01 | 0.850D+01 | 0.103D+02 | 0.114D+02 |
| $2^{-6}$ | 0.516D+01 | 0.785D+01 | 0.990D+01 | 0.137D+02 | 0.165D+02 | 0.182D+02 |
| $2^{-7}$ | 0.516D+01 | 0.795D+01 | 0.120D+02 | 0.188D+02 | 0.255D+02 | 0.289D+02 |
| $2^{-8}$ | 0.516D+01 | 0.795D+01 | 0.120D+02 | 0.188D+02 | 0.255D+02 | 0.315D+02 |
| $2^{-9}$ | 0.516D+01 | 0.795D+01 | 0.120D+02 | 0.188D+02 | 0.255D+02 | 0.315D+02 |
| $2^{-10}$ | 0.516D+01 | 0.795D+01 | 0.120D+02 | 0.188D+02 | 0.255D+02 | 0.315D+02 |
| $R_{\text{unif}}^N$ | −0.62 | −0.60 | −0.65 | −0.44 | −0.30 | |

Table VII. Maximum pointwise errors, $\|D_x^- V_v - v_x\|_{\tilde{\Omega}_v^N} / \|V_v\|_{\tilde{\Omega}_v^N}$, computed on the sub-domain $\tilde{\Omega}_v^N$, for various values of $v$ and $N$.

| | Number of intervals $N$ | | | | | |
|---|---|---|---|---|---|---|
| $v$ | 32 | 64 | 128 | 256 | 512 | 1024 |
| 1 | 0.225D+01 | 0.132D+01 | 0.718D+00 | 0.356D+00 | 0.177D+00 | 0.895D−01 |
| $2^{-1}$ | 0.926D+00 | 0.538D+00 | 0.292D+00 | 0.149D+00 | 0.754D−01 | 0.381D−01 |
| $2^{-2}$ | 0.731D+00 | 0.433D+00 | 0.237D+00 | 0.120D+00 | 0.601D−01 | 0.304D−01 |
| $2^{-3}$ | 0.776D+00 | 0.464D+00 | 0.254D+00 | 0.129D+00 | 0.648D−01 | 0.328D−01 |
| $2^{-4}$ | 0.879D+00 | 0.537D+00 | 0.297D+00 | 0.150D+00 | 0.757D−01 | 0.383D−01 |
| $2^{-5}$ | 0.104D+01 | 0.656D+00 | 0.367D+00 | 0.185D+00 | 0.933D−01 | 0.473D−01 |
| $2^{-6}$ | 0.115D+01 | 0.829D+00 | 0.468D+00 | 0.239D+00 | 0.122D+00 | 0.621D−01 |
| $2^{-7}$ | 0.115D+01 | 0.826D+00 | 0.525D+00 | 0.295D+00 | 0.164D+00 | 0.857D−01 |
| $2^{-8}$ | 0.115D+01 | 0.826D+00 | 0.525D+00 | 0.295D+00 | 0.164D+00 | 0.915D−01 |
| $2^{-9}$ | 0.115D+01 | 0.826D+00 | 0.525D+00 | 0.295D+00 | 0.164D+00 | 0.915D−01 |
| $2^{-10}$ | 0.115D+01 | 0.826D+00 | 0.525D+00 | 0.295D+00 | 0.164D+00 | 0.915D−01 |
| $R_{\text{unif}}^N$ | 0.78 | 0.88 | 1.01 | 1.01 | 0.95 | |

of the errors is obtained by dividing the maximum absolute error in each instance by the maximum absolute value of $V_v$.

Notice that along the rows the errors are increasing which leads to the negative rates in Table VI. This behaviour would seem to indicate that computation of this derivative is difficult near $\Gamma_L$. To see whether we can compute the derivative accurately anywhere in the domain,

 

we consider the errors on the sub-domain $\tilde{\Omega}_v^{\mathbf{N}} = \bar{\Omega}_v^{\mathbf{N}} \cap (0.2, 1.1] \times [0, 1]$. The results in Table VII verify that the larger errors occur in the vicinity of $\Gamma_{\mathrm{L}}$ and that $v$-convergence for the scaled approximation to $v_x$ is only achievable on a subdomain.

Note again that the range of values of the perturbation parameter, $v$, that has been considered in the preceding sections, is not physically valid. The laminar jet exists and remains non-turbulent for values of $v \approx 2^{-4}$ [5]. Our reason for choosing values of $v$ outside the physical range is to put our numerical method through a rigorous test.

Also, the value of $a$ reflects how far we are from the source. From a physical point of view it is appropriate to choose $a$ such that we are far from the source. Our choice of $a$ in the preceding sections has been to stay close to the source. The reason for this rests with the fact that the problem serves as a challenging model to test our theories on, but only when we stay close to the singularity. It has been suggested that the distance from the source should be some function of $v$, i.e. $a$ should be a function of $v$. We have noted that $a = 1/v$ seems to give solutions that are $v$-uniform convergent and do not require the use of the stabilization parameters $\theta_1$ and $\theta_2$. As already mentioned, there is no difficulty in solving the problem in this case because of the insignificance of the boundary layer; i.e. in fact the problem can also be solved on a uniform mesh, however, the results are less accurate.

## 6. CONSERVATION OF MOMENTUM

At the beginning of this paper, it was noted that there is a requirement of conservation of the momentum in the $x$ direction, i.e. for each $x$,

$$\int_{-\infty}^{\infty} \rho u^2 \, \mathrm{d}y = J_0 = \text{constant} \tag{13}$$

where $J_0 = 1$ for the purpose of all our results. We now examine some computed approximations of integral (13). Note that, as this problem is symmetric about the jet axis ($y = 0$), and since $\rho = J_0 = 1$,

$$\int_{0}^{\infty} u^2 \, \mathrm{d}y = \tfrac{1}{2} \tag{14}$$

Some sources of error in the approximation of (14) are evident. The domain of numerical solution is $[0, 1]$, so we can actually only approximate $\int_0^1 u^2 \, \mathrm{d}y$. As the numerical method is non-conservative, some loss of conservation is also expected, in particular as $x$ increases, since the jet then spreads out. We will approximate the integral using Romberg's method with the tolerance set to $10^{-6}$. Table VIII shows the approximation of (14) at the left boundary $\Gamma_{\mathrm{L}}$. These values are quite close to the actual value of 0.5 and, in fact, as $N \to \infty$ the computed loss of conservation tends to zero, and more quickly if $v \to 0$.

Table IX shows the approximation of (14) at the right boundary $\Gamma_{\mathrm{R}}$; here we notice that the values, as anticipated, are smaller than the values at the left boundary. However, for large $N$ and reasonably, small $v$, the loss of computed momentum is small. The fact that the computational domain is finite strongly influences the computations for $v = 1$, where the spread of the jet outside the computational domain is most significant.

 

Table VIII. The approximation of integral (14) at the left boundary $\Gamma_L$.

| | Number of intervals $N$ | | | | | |
|---|---|---|---|---|---|---|
| $v$ | 32 | 64 | 128 | 256 | 512 | 1024 |
| 1 | 0.453D+00 | 0.469D+00 | 0.477D+00 | 0.481D+00 | 0.483D+00 | 0.484D+00 |
| $2^{-4}$ | 0.484D+00 | 0.495D+00 | 0.499D+00 | 0.500D+00 | 0.500D+00 | 0.500D+00 |
| $2^{-8}$ | 0.466D+00 | 0.486D+00 | 0.495D+00 | 0.498D+00 | 0.500D+00 | 0.500D+00 |
| $2^{-12}$ | 0.466D+00 | 0.486D+00 | 0.495D+00 | 0.498D+00 | 0.500D+00 | 0.500D+00 |
| $2^{-16}$ | 0.466D+00 | 0.486D+00 | 0.495D+00 | 0.498D+00 | 0.500D+00 | 0.500D+00 |
| $2^{-20}$ | 0.466D+00 | 0.486D+00 | 0.495D+00 | 0.498D+00 | 0.500D+00 | 0.500D+00 |

Table IX. The approximation of integral (14) at the right boundary $\Gamma_R$.

| | Number of intervals $N$ | | | | | |
|---|---|---|---|---|---|---|
| $v$ | 32 | 64 | 128 | 256 | 512 | 1024 |
| 1 | 0.180D+00 | 0.183D+00 | 0.184D+00 | 0.185D+00 | 0.185D+00 | 0.185D+00 |
| $2^{-4}$ | 0.420D+00 | 0.456D+00 | 0.476D+00 | 0.486D+00 | 0.491D+00 | 0.494D+00 |
| $2^{-8}$ | 0.384D+00 | 0.426D+00 | 0.459D+00 | 0.477D+00 | 0.487D+00 | 0.493D+00 |
| $2^{-12}$ | 0.381D+00 | 0.429D+00 | 0.459D+00 | 0.477D+00 | 0.487D+00 | 0.493D+00 |
| $2^{-16}$ | 0.375D+00 | 0.426D+00 | 0.458D+00 | 0.477D+00 | 0.487D+00 | 0.493D+00 |
| $2^{-20}$ | 0.371D+00 | 0.424D+00 | 0.457D+00 | 0.476D+00 | 0.487D+00 | 0.493D+00 |

## 7. SUMMARY

We have demonstrated computationally that the numerical method (10)–(11) and associated algorithm (12) gives solutions for the velocity terms and their scaled discrete derivatives which appear to be uniformly convergent with respect to the viscosity $v$. The number of iterations of the algorithm is also independent of the perturbation parameter $v$. We have considered also the issue of conservation of the momentum for each $x$ and noted that, since our method is not taking the conservation into account explicitly, some momentum is lost at the right boundary $\Gamma_R$. However, for small $v$ and large $N$ the momentum is reasonably conserved.

ACKNOWLEDGEMENTS

This work was supported in part by the Enterprise Ireland Grants SC-97-612 and SC-98-612 and by the Russian Foundation for Basic Research Grant No. 01-01-01022.

REFERENCES

1. Hegarty AF, Miller JJH, O'Riordan E, Shishkin GI. Special meshes for finite difference approximations to an advection-diffusion equation with parabolic layers. *Journal of Computational Physics* 1995; **117**:47–54.
2. Miller JJH, O'Riordan E, Shishkin GI. *Fitted Numerical Methods for Singular Perturbation Problems*. World Scientific: London, 1996.
3. Farrell PA, Hegarty AF, Miller JJH, O'Riordan E, Shishkin GI. *Robust Computational Techniques for Boundary Layers*. Chapman & Hall/CRC Press: Boca Raton, 2000.

 

4. Prandtl L, Tietjens OG. *Applied Hydro- and Aeromechanics*. Dover Publications: New York, 1957.
5. Schlichting H. *Boundary-layer Theory* (7th edn). McGraw-Hill: New York, 1979.
6. Acheson DJ. *Elementary Fluid Dynamics*. Oxford University Press: Oxford, 1990.
7. Warsi ZUA. *Fluid Dynamics*: *Theoretical and Computational Approaches*. CRC Press: Boca Raton, 1993.
8. Ansari AR. On the use of Shishkin meshes to obtain parameter robust numerical solutions of singularly perturbed differential equations. *Ph.D. Thesis*, Department of Mathematics & Statistics, University of Limerick, Limerick, Ireland, 2001.

 